Acta Pharmaceutica Sinica B 2023;13(9):3694–3707

Chinese Pharmaceutical Association
Institute of Materia Medica, Chinese Academy of Medical Sciences

Acta Pharmaceutica Sinica B

www.elsevier.com/locate/apsb
www.sciencedirect.com

ORIGINAL ARTICLE

Predicting and overcoming resistance to CDK9 inhibitors for cancer therapy

Chen Hu[a,c,†], Lijuan Shen[a,b,†], Fengming Zou[a,c,†], Yun Wu[a,c,†], Beilei Wang[a,c], Aoli Wang[a,c], Chao Wu[d], Li Wang[a,c], Jing Liu[a,b,c,*], Wenchao Wang[a,b,c,*], Qingsong Liu[a,b,c,e,*]

[a]*Anhui Province Key Laboratory of Medical Physics and Technology, Institute of Health and Medical Technology, Hefei Institutes of Physical Science, Chinese Academy of Sciences, Hefei 230031, China*
[b]*University of Science and Technology of China, Hefei 230026, China*
[c]*Hefei Cancer Hospital, Chinese Academy of Sciences, Hefei 230031, China*
[d]*Tarapeutics Science Inc., Bengbu 233000, China*
[e]*Precision Medicine Research Laboratory of Anhui Province, Hefei 230088, China*

Received 15 March 2023; received in revised form 19 April 2023; accepted 22 May 2023

KEY WORDS

Acquired resistance mutations;
CDK9 inhibitors;
Transcription;
Single nucleotide polymorphisms;
BAY1251152

Abstract Abnormally activated CDK9 participates in the super-enhancer mediated transcription of short-lived proteins required for cancer cell survival. Targeting CDK9 has shown potent anti-tumor activity in clinical trials among different cancers. However, the study and knowledge on drug resistance to CDK9 inhibitors are very limited. In this study, we established an AML cell line with acquired resistance to a highly selective CDK9 inhibitor BAY1251152. Through genomic sequencing, we identified in the kinase domain of CDK9 a mutation L156F, which is also a coding SNP in the CDK9 gene. By knocking in L156F into cancer cells using CRISPR/Cas9, we found that single CDK9 L156F could drive the resistance to CDK9 inhibitors, not only ATP competitive inhibitor but also PROTAC degrader. Mechanistically, CDK9 L156F disrupts the binding with inhibitors due to steric hindrance, further, the mutation affects the thermal stability and catalytic activity of CDK9 protein. To overcome the drug resistance mediated by the CDK9-L156F mutation, we discovered a compound, IHMT-CDK9-36 which showed potent inhibition activity both for CDK9 WT and L156F mutant. Together, we report a novel resistance mechanism for CDK9 inhibitors and provide a novel chemical scaffold for the future development of CDK9 inhibitors.

*Corresponding authors.
E-mail addresses: jingliu@hmfl.ac.cn (Jing Liu), wwcbox@hmfl.ac.cn (Wenchao Wang), qsliu97@hmfl.ac.cn (Qingsong Liu).
[†]These authors made equal contributions to this work.
Peer review under the responsibility of Chinese Pharmaceutical Association and Institute of Materia Medica, Chinese Academy of Medical Sciences.

https://doi.org/10.1016/j.apsb.2023.05.026

1. Introduction

Cyclin-dependent protein kinases (CDKs) are serine/threonine kinases belonging to CMGC subfamily of the human kinome[1] and play crucial regulatory roles in multiple physiological processes in cells, including cell cycle, proliferation, transcription, and metabolism[1,2]. Dysregulation of CDK kinases contributes to cancer progression by unscheduled cell cycle and uncontrolled gene expression[3]. Targeting deregulated CDKs has shown potent therapeutic efficacy in clinical cancer therapy, such as selective CDK4/6 inhibitors Palbociclib and Ribociclib, which have been approved by US Food and Drug Administration (FDA) for HR+ and HER2− breast cancers[4,5]. CDK9-cyclin T1 is the catalytic subunit in positive transcription elongation factor b complex (P-TEFb), which phosphorylates the RNA polymerase II CTD at Ser2 and regulates transcription elongation[6,7]. In cancers, abnormally activated CDK9 participates the super-enhancer mediated transcription of short-lived proteins required for cancer cell survival, such as MCL1 and MYC[8]. This transcription addiction makes the cancer cells more sensitive to CDK9 suppression, which has shown potent anti-tumor efficacy in pre-clinical tumor models by inducing MCL1 decrease and cell apoptosis[7,9]. Promising data from preclinical studies urged the launching of a race for the development of potent CDK9 inhibitors and some of them are being tested in clinical trials[4,10−12]. Due to toxicity and adverse effects as the result of pan-CDK inhibition activity, the development of first-generation CDK9 inhibitors has been hindered, such as Alvocidib and Dinaciclib[13]. However, with increased selectivity over other CDK kinases, the second-generation inhibitors, such as BAY1251152 and AZD4573, are currently being evaluated in clinical trials in patients with solid tumors and hematological malignancies with better safety profiles[13,14].

In spite of the encouraging development of CDK9 inhibitors in cancer therapy, little is known about the possible mechanisms that could lead to resistance to these inhibitors. Just like any other kinase inhibitors that are in clinical application and evaluation[15], CDK9 inhibitors would probably be challenged by various acquired resistances with prolonged drug treatment. The most common drug resistance mechanisms seen with kinase inhibitors include secondary mutations in the catalytic domains of the targeted kinases and re-routing of alternative signaling pathways[16]. Understanding of those drug resistance mechanisms is crucial for the development of the next-generation CDK9 inhibitors that are able to overcome the predicted resistance. However, because none of the current CDK9 inhibitors has been approved for clinical use yet, the study and knowledge related to drug resistance are very limited, since now only ubiquitin ligase CUL5 has reported mediating the resistance to CDK9 and MCL1 inhibitors[17].

Single nucleotide polymorphisms (SNP) are the most abundant type of genetic variation in human genome[18]. The SNPs in protein-coding regions lead to non-synonymous mutations, which may induce the misfold, instability, inactivation or dysfunction of proteins and then induce diseases[19]. For example, a SNP in the β-globin gene, which results in glutamate being substituted by valine at position 6 in the amino acid sequence, induce sickle cell anemia that is associated with high morbidity and mortality[20]. During the last decade, thanks to genome-wide association studies (GWAS) and the large-scale next-generation genomic sequencing in cancer patients, many kinase SNPs are reported to be associated with susceptibility to cancers, cancer outcomes, or responses to cancer therapy[21−24].

In this report, as an initial effort to characterize the potential acquired resistance mechanisms to CDK9 inhibitors, we constructed an AML cell line resistant to a highly selective CDK9 inhibitor BAY1251152, and identified the resistant mutation as a point mutation in the CDK9 kinase domain, L156F. Database search showed that the mutation we found in the resistant cell line is a rare coding SNP (rs1158106390). Using CRISPR/Cas9 technology, we found that targeted gene editing of this SNP is sufficient to render cells resistant to CDK9 inhibitors. The mutation impairs the binding of inhibitors to CDK9 due to steric hindrance and influences the CDK9 kinase catalytic activity. Through high-throughput screening, we also discovered a novel chemical scaffold of IHMT-CDK9-36, that is able to overcome the drug resistance mediated by the CDK9-L156F mutation. Together, our findings report the first drug-resistant mutation against CDK9 inhibitor, which is also a rare SNP, and we provide a new chemical scaffold that can overcome this resistance for future development of CDK9 inhibitors.

2. Materials and methods

2.1. Cell culture, cell growth inhibition assay and apoptosis assay

The human cancer cell lines MOLM13 were provided by Dr. Scott Armstrong, Dana-Farber Cancer Institute (DFCI), Boston, MA, USA. MOLM13 was cultured with RPMI medium with 10% FBS. HeLa, MCF7 cells were obtained from COBIOER (Nanjing, China) and cultured in DMEM medium with 10% certified fetal bovine serum (C0400, VivaCell, Shanghai, China). Briefly, cells were seeded in 96-well plates and treated with serially diluted compounds. Then, CellCounting-Lite 2.0 (#DD1101-02, Vazyme, Nanjing, China) was added to evaluate the cell viability. The cell apoptosis was detected by Annexin V-FITC/PI Apoptosis Detection Kit (A211, Vazyme, China). Briefly, the cells were collected and washed with cold PBS twice. After staining by annexin V-FITC and PI staining solution, the cells were analyzed by flow cytometry (CytoFLEX, BECKMAN).

2.2. Reagents and antibodies

Compounds BAY1251152, AZD4573 and JSH-009 were purchased from MedChemexpress (Shanghai, China). RNA polymerase II CTD peptide YSPTSPS was synthesized by GL Biochem (Shanghai, China). Anti-PPP1A/PPP1CA (phosphoT320) (#ab62334), anti-RNA polymerase II Ser2 (#ab193468), Ser5 (#ab240740) and anti-RNA polymerase II antibody (#ab264350) were purchased from Abcam (Cambridge, MA,

USA); c-Myc antibody (#5605), PARP antibody (#9532), Mcl-1 antibody (#94296), phospho-Rb (Ser780) (#9307), total Rb (#9309) and caspase3 antibody (#9665) were purchased from Cell Signaling Technology (Danvers, MA, USA). PPP1CA antibody (67070-1-Ig) and GAPDH (60004-1-Ig) were purchased from Proteintech (Wuhan, China).

2.3. BAY1251152 resistant cell generation

MOLM13 cells were cultured in 1640 medium with 20 nmol/L BAY1251152 initially, then the survival cells were isolated and treated with gradual dose escalation of BAY1251152 up to 1 μmol/L. Then stable resistance clones were screened by infinite dilution and cultured in medium without BAY1251152. And the BAY1251152 resistance potency of clones was determined by anti-proliferation assay with CellCounting-Lite 2.0 reagent.

2.4. CDK9 L156F knock-in cell line generation

Guide RNA target CDK9 was designed and cloned into PX459, and donor DNA for CDK9 L156F knock-in was synthesized by General Biol. HeLa cells were co-transfected by sgRNA-PX459 and donor DNA (1 μg:1 μg), and selected by puromycin for 48 h. Then single cell clones were obtained by infinite dilution. The CDK9 KI cells were analyzed by genomic DNA PCR and sequencing.

2.5. RNA sequencing and differential expression analysis

Transcriptome sequencing of MOLM13/MOLM13-BR cells was performed using the Illumina Novaseq 6000 in LC-Bio (Hangzhou, China). Genes differential expression analysis was performed by DESeq2 software between two different groups (and by edgeR between two samples). The genes with the parameter of false discovery rate (FDR) below 0.05 and absolute fold change $\geq$2 were considered differentially expressed genes[25].

2.6. Real-time RT-PCR

After drug treatment, the total RNA was extracted by SPARKeasy Cell RNA Kit (AC0205, Shandong Sparkjade Biotechnology Co., Ltd.). cDNA samples were prepared by reverse transcription with Hifair® V one-step RT-gDNA digestion SuperMix for qPCR (11142ES60, Yeason, China), and MCL1/MYC mRNA levels were detected by Hieff® qPCR SYBR Green Master Mix (11201ES08, Yeason, China).

PCR Primers used for real-time PCR

MCL1: GCTGGGATGGGTTTGTGGAGT; GCCAAACCAGCTCC TACTCCA.

MYC: CCTGGTGCTCCATGAGGAGAC; CAGACTCTGA CCTTTTGCCAGG.

GAPDH: TGGTCACCAGGGCTGCTTTTA; TTCCCGTTCT CAGCCTTGACG.

2.7. Protein purification

CyclinT1 (1−298) coding fragment was cloned into pET28A with an N-terminal GST tag, and purified by GSH resins. Full-length CDK9 WT and L156F gene fragments were constructed in p-FASTBAC HTA vector (Invitrogen), and SF9 were transfected of CDK9 bacmids for the baculovirus package. Briefly, the SF9 cells were collected after 48 h infection of CDK9 baculovirus. Cells were sonicated and the suspension was loaded to Ni-NTA Column (QIAGEN, 1018244). Then the proteins were step eluted with buffer containing 250 mmol/L imidazole. The eluted CDK9 proteins were mixed with cyclinT1 proteins and loaded on a Superdex-200 column equilibrated in 50 mmol/L Tris pH 8.0, 500 mmol/L NaCl, 1 mmol/L DTT. Peak fractions were concentrated and used for *in vitro* kinase assay and binding affinity test.

2.8. In vitro kinase assay

To determine the inhibition activity of compounds, CDK9/cyclinT1 proteins were incubated with the gradient diluted compound for 30 min at room temperature. Then, 200 μmol/L RNA polymerase CTD peptide substrate and 10 μmol/L ATP mixtures were added and reacted at room temperature for 0.5 h. The ADP produced in the reaction was detected by the ADP-Glo assay from Promega. Briefly, add 10 μL ADP-Glo™ Reagent to the reaction and incubate for 40 min. Then 20 μL Kinase Detection Reagent to reaction and incubate for 30−60 min. The luminescence was measured with a plate reader ENVISION, PerkinElmer (Waltham, MA, USA). Each sample was assembled as follows:

Sample	10 μL/sample
CDK9/cyclin T1 protein	4 μL
CTD/ATP mix	5 μL
Inhibitor (in 5% DMSO buffer)	1 μL

For kinetic parameters measurement, the CDK9 proteins were incubated with saturated RNA Pol II CTD peptide and gradient diluted ATP for 20 min at room temperature, then ADP produced in the reaction was detected by the ADP-Glo reagent. The IC_{50} of compounds and kinetic parameters of kinases were fitted by GraphPad Prism8.0 software.

2.9. Micro-scale thermophoresis assay

10 μmol/L CDK9/cyclinT1 complex proteins were labeled by RED-NHS protein label KIT (MO-L011, Nano-Temper). The labeled protein was diluted to 20 nmol/L with 20 mmol/L Tris, 150 mmol/L NaCl, pH 7.5 buffer. 10 μL proteins were incubated with 10 μL serial dilution of compounds at room temperature for 30 min. Then the mixture was loaded to capillary supplied by Nano-Temper and thermophoresis was scanned by Monolith (Nano-Temper). The equilibrium dissociation constants were calculated by MO.affinity Analysis software.

2.10. Xenograft tumor models

Five-week-old female Balb/c nude mice were purchased from GemPharmatech Co., Ltd. (Nanjing, China). All animals were housed in a specific pathogen-free facility and used according to the animal care regulations of Hefei Institutes of Physical Science Chinese Academy of Sciences. Prior to implantation, cells were harvested during exponential growth phase. 8 million MOLM13/MOLM13-BR cells in 1640 medium were formulated as a 1:1

mixture with Matrigel (BD Biosciences) and injected into the subcutaneous space on the right flank of nude mice. Animals were then randomized into treatment groups for the efficacy study. IHMT-CDK9-36 (8 mg/kg) and BAY1251152 (8 mg/kg) were delivered every two days in a solution (5% DMSO, 20% Solutol HS-15 in ddH_2O) by intravenous injection. Body weight and tumor growth were measured every two days after drug treatment. Tumor volumes were calculated as Eq. (1):

$$\text{Tumor volume}\left(\text{mm}^3\right) = [(W_2 \times L)/2] \quad (1)$$

where width (W) is defined as the smaller of the two measurements and length (L) is defined as the larger of the two measurements.

2.11. Statistical analysis

Statistical significance was defined as a P value using the appropriate statistical test method. Error bars are presented as means ± standard deviation (SD). Statistical analyses were performed using Prism software (GraphPad 8.0).

3. Results

3.1. Construction of drug-resistant cell line to a selective CDK9 inhibitor

Since CDK9 inhibitors are still being tested in clinical trials, we intended to investigate the possible resistance mechanism for CDK9 using *in vitro* cell line models. First, to avoid the off-target effect induced by targeting other CDKs or kinases, we chose a highly selective CDK9 inhibitor BAY1251152 as the tool compound. Since BAY1251152 is under clinical trial for hematological malignancies and advanced blood cancer, we chose a BAY1251152-sensitive AML cell line MOLM13 to develop an acquired resistance model. MOLM13 cells were continuously cultured in medium with gradual dose escalation of BAY1251152 and finally maintained in 1 μmol/L BAY1251152 for 4 weeks. Stable resistance clones were then screened by infinite dilution and cultured in medium without BAY1251152 (Fig. 1A). The anti-proliferation activity of BAY1251152 against these resistant clones were measured after 24 h of treatment. Among these clones, MOLM13-BR cell clone (BR denoted as BAY1251152 resistance) showed the highest resistance with GI_{50} (50% growth inhibition) = 1050 nmol/L, while the GI_{50} against parental MOLM13 was only 93.76 nmol/L (Fig. 1B). Through continuous monitoring the cell viability of MOLM13 and MOLM13-BR cells in 8 days, we found that the growth rate of MOLM13-BR cells was slightly slower than parental MOLM13, and a medium dose of 100 nmol/L BAY1251152 reduced the cell viability in MOLM13 cells but not in MOLM13-BR cells (Fig. 1C). Meanwhile, the anti-tumor efficacy of BAY1251152 was evaluated in mouse xenograft models inoculated with MOLM13 or MOLM13-BR cells. Consistent with our *in vitro* results, tumors derived from MOLM13-BR cells also exhibited resistance to BAY1251152 (Fig. 1D, Supporting Information Fig. S1).

To verify that the drug resistance in MOLM13-BR is mediated through the CDK9 signaling pathway, we then investigated CDK9-related transcription activity in MOLM13 and MOLM13-BR cell lines. First, the differential transcriptomic analysis showed that the total number of down-regulated genes by BAY1251152 was reduced in MOLM13-BR cells (Supporting Information Fig. S2). In particular, upon BAY1251152 treatment, the transcription levels of the anti-apoptosis factor MCL1 and survival-related gene MYC underwent dramatic changes in MOLM13, which showed no significant change in MOLM13-BR cells (Fig. 2A). The reduced suppression by BAY1251152 on MCL1/MYC transcription in MOLM13-BR cells was also validated by real-time RT-PCR (Fig. 2B). We then validated the transcriptomic result by examining the inhibition potency of BAY1251152 on the phosphorylation of RNA Pol II CTD Ser2 and the protein level of MCL1/MYC, which also significantly attenuated in MOLM13-BR cells (Fig. 2C), suggesting that the relatively abundant MCL1/MYC helps to protect the resistance cells from undergoing apoptosis, which is seen with parental MOLM13 cells (Fig. 2D). Taken together, we obtained an acquired resistant cell line to BAY1251152 mediating through the CDK9 signal pathway, and it is no longer sensitive to BAY1251152 either *in vitro* or *in vivo*.

3.2. Resistance to CDK9 inhibitor is conferred by CDK9 L156F mutation

To identify the resistance mechanism in MOLM13-BR cells, we first compared the genome of MOLM13-BR cells with parental MOLM13 by whole exome sequencing, in which a point mutation was identified in CDK9 coding region only in MOLM13-BR cells but not parental MOLM13 cells (Fig. 3A). Subsequent Sanger sequencing confirmed the mutation is a C>T substitution in MOLM13-BR CDK9 gene sequence, which results in an amino acid substitution from leucine (CTT) to phenylalanine (TTT) of residue 156 located in the beta-sheet just after the catalytic loop in the c-lobe of CDK9 (Fig. 3B).

To investigate whether CDK9 L156F is the driving force in the development of resistance to BAY1251152, we introduced L156F mutation into the CDK9 gene using CRISPR/Cas9-mediated genomic editing in HeLa cells, which is sensitive to CDK9 inhibitor BAY1251152 as we previously confirmed. Through genomic DNA sequencing and allele separation, we validated that in the edited HeLa cells, one CDK9 gene allele was modified into TTT at residue 156 for phenylalanine, while the other allele has a nonsense mutation (TGA) (Fig. 3C). Then cell viability of HeLa and HeLa-CDK9-L156F was measured after exposure to BAY1251152 for 24 h. As the result showed, BAY1251152 suppressed HeLa cells viability effectively (GI_{50} = 45 nmol/L), while the suppression vanished in HeLa-CDK9-L156F cells (Fig. 3D). Consistent with cell viability result, BAY1251152 inhibition on p-Ser2 RNA Pol II CTD phosphorylation in HeLa-CDK9-L156F cells attenuated significantly, which is accompanied by reduced suppression on MYC/MCL1 expression (Fig. 3E and F). Meanwhile, PARP and caspase3 cleavage was also reduced in HeLa-CDK9-L156F cells, suggesting that less apoptosis is induced by BAY1251152 in resistant cells upon drug treatment (Fig. 3E). Based on the above results from two different cancer cell lines with L156F mutation, we concluded that CDK9 L156F mutation is the driven force responsible for the acquired resistance to BAY1251152.

To investigate whether L156F is a common resistance mechanism of CDK9 inhibitors, we tested another two CDK9 inhibitors AZD4573 (ATP-competitive) and THAL-SNS-032 (PROTAC agent able to degrade CDK9 protein). After 24-h treatment, the anti-proliferation activities of both AZD4573 and THAL-SNS-032 decreased by 3- and 8-fold in MOLM13-BR cells, respectively (Fig. 4A). Meanwhile, the ability of CDK9 degradation by THAL-

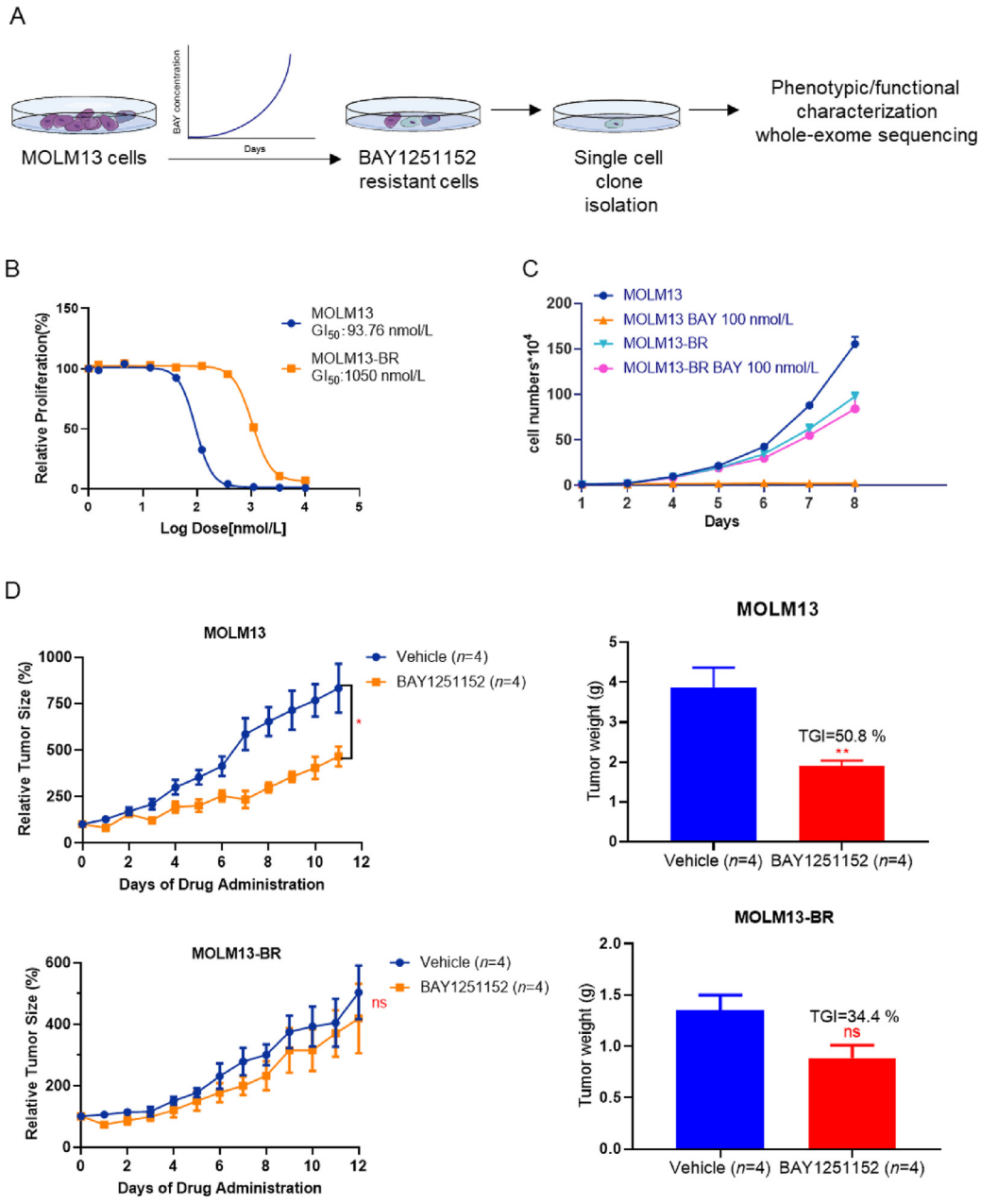

Figure 1 Acquired resistance to CDK9 inhibitor BAY1251152. (A) Schematically graph of the generation of BAY1251152 resistance cell line. MOLM13 cells were cultured in medium with gradient dose escalation of BAY1251152. (B) The anti-proliferation activities of BAY1251152 against parental MOLM13 and MOLM13-BR cell lines were measured by Cell Titer-Glo. (C) The cell viability of parental MOLM13 and MOLM13-BR cell lines monitored for 8 days with or without BAY1251152. (D) The tumor growth inhibition efficacy of 5 mg/kg/Q2D BAY1251152 administrated by intravenous injection in mouse engraftment models inoculated with MOLM13 or MOLM13-BR cells (n = 4/group). Results in the graphs are expressed as means ± SD. *P-value < 0.05, **P-value < 0.01 ns, not significant.

SNS-032 also decreased in MOLM13-BR cells (Fig. 4B). Next, we examined the influence of L156F mutant on drug sensitivity by *in vitro* ADP-Glo assay. Consistent with our cellular results, the inhibitory potency of BAY1251152 and AZD4573 were both attenuated by the L156F mutation (Fig. 4C), moreover, the equilibrium dissociation constants K_d measured by micro thermophoresis also showed that the binding affinity of BAY1251152 and AZD4573 were disrupted by the mutation (Fig. 4D and E). These results indicated that L156F could be a general resistance mechanism for CDK9 inhibitors.

3.3. L156F is a rare coding SNP resulting in reduced CDK9 kinase activity

We next searched this mutation in genetic databases, including COSMIC and GENIE, and we found no report on this mutation. However, through analysis of the single nucleotide polymorphisms (dbSNP) database, we found a rare SNP rs1158106390 in the CDK9 gene on chromosome 9 that causes the same missense variation. The SNP causes allele changes as either C > T or C > A, which result in amino acid substitutions as F156(TTT)

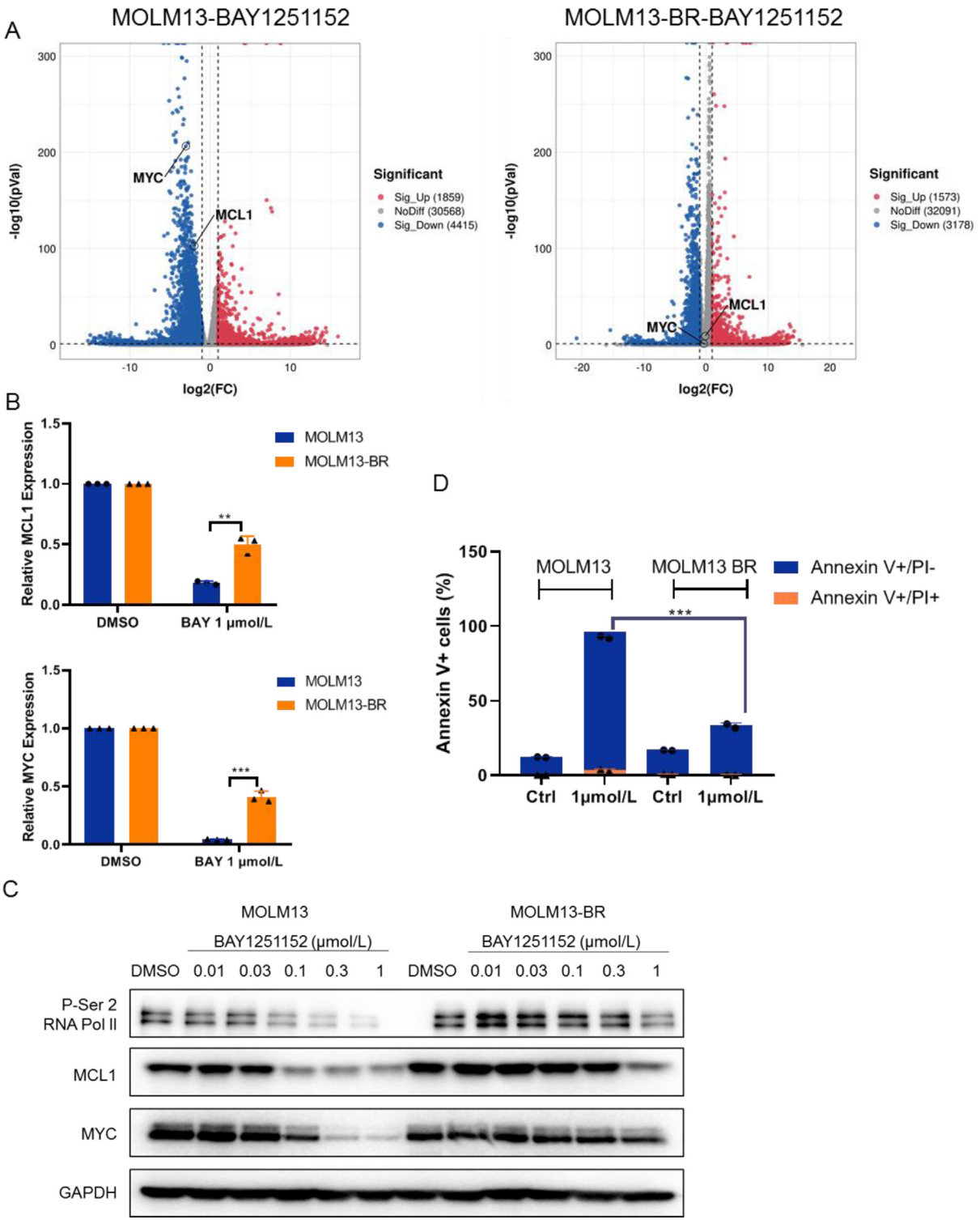

Figure 2 CDK9 signaling pathway mediates drug resistance to BAY1251152. (A) The volcano map of differential transcriptomic analysis treated with 1 μmol/L BAY12515521 for 3 h in MOLM13 (left) and MOLM13-BR cells (right). Changes in transcript are defined as not significant (gray), significant up-regulate (red), significant down-regulate (blue). (B) The transcription suppression efficiency of BAY1251152 in MOLM13 and MOLM13-BR cell lines were detected by real time RT-PCR. (C) The effect on phosphorylation of RNA Pol II and MYC/MCL were detected by Western-blot after 3 h treatment. (D) Apoptosis in MOLM13 and MOLM13-BR cell lines measured by Annexin V/PI dual strain assay after 24 h treatment of BAY1251152. Results in the graphs are expressed as means ± SD. ***P*-value < 0.01, ****P*-value < 0.001.

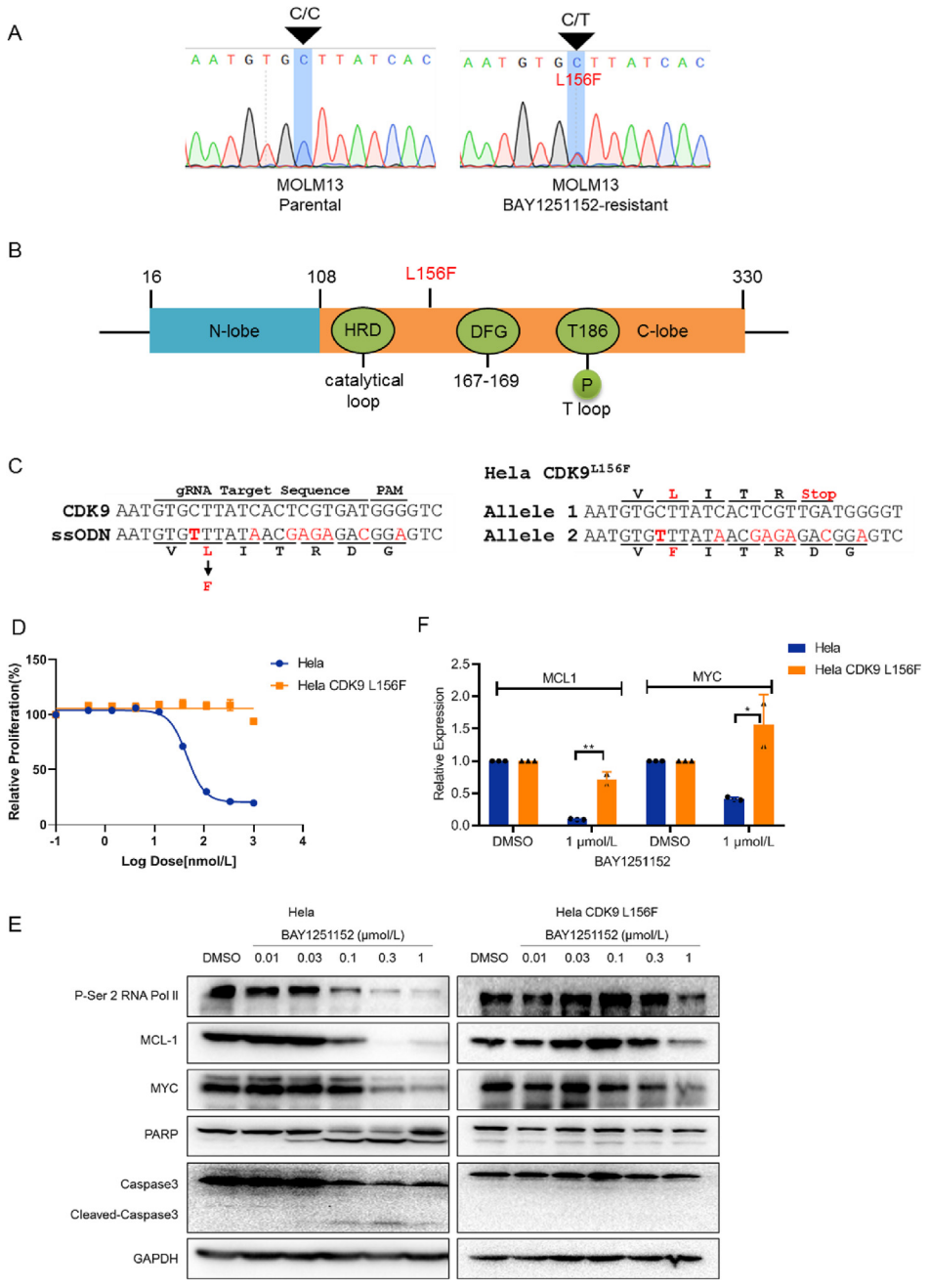

Figure 3 CDK9-F156 associated with BAY1251152 resistance. (A) The genotypes of resistance cell line were analyzed by whole exome sequencing and CDK9 mutation was validated by sanger sequencing. (B) Schematic of the CDK9 protein is shown with both the protein domains and the position of the L156F mutation. (C) CDK9 L156F mutation was induced into HeLa through CRISRP-Cas9 mediated HDR. Left is the template ssODN sequence and right is the edited genomic sequence of CDK9 in HeLa cells. (D) The effect of BAY1251152 on cell viability was evaluated by cell Titer-Glo assay in parental HeLa and HeLa CDK9 L156F cells for 24 h. (E) Immunoblot of CDK9 downstream regulated proteins and cleavage of PARP and caspace3 after BAY1251152 treatment at the concentrations indicated for 24 h. (F) Changes of MCL1/MYC gene expression levels in HeLa and HeLa CDK9 L156F cells after treatment with 1 μmol/L BAY1251152 for 6 h. Results in the graphs are expressed as means ± SD. **P*-value < 0.05, ***P*-value < 0.01.

or I156(ATT) with no reported clinical significance (Fig. 5A). Since many SNPs are reported to be associated with drug sensitivity, this SNP could be a predictive biomarker for CDK9 inhibitor sensitivity in clinic application.

Structural analysis using available CDK9 protein crystallography data revealed that, current CDK9 inhibitors occupy the ATP-binding pocket that is sandwiched between Ala46 (located in N-lobe) and Leu156 (located in the β-sheet just after the catalytical loop, PDB ID:6z45). Leu156 is located in close vicinity with its side chain pointing to the ATP-binding pocket (Supporting information Fig. S3A). Therefore, we hypothesized that the bulky phenylalanine side chain in the L156F mutation might abrogate the binding of inhibitors to CDK9 protein due to steric hindrance. To support our hypothesis, we performed computer-aided

A

	GI_{50} (nmol/L)		DRI
	MOLM13	MOLM13-BR	
AZD4573	4.056	12.31	3.1
THAL-SNS-032	63.00	482.1	7.7

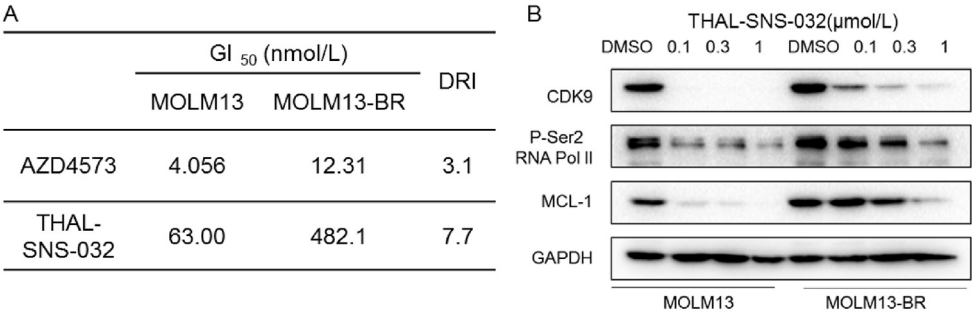

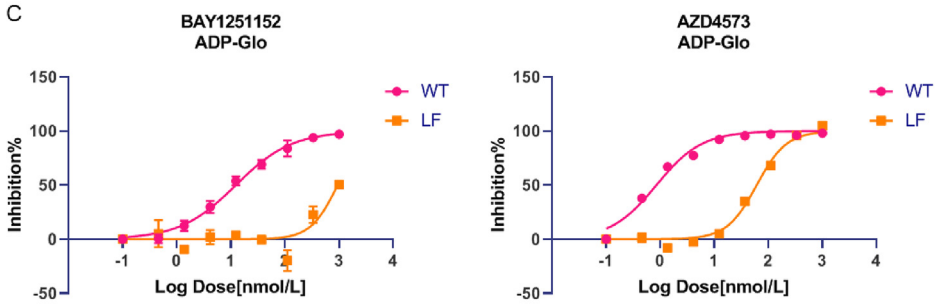

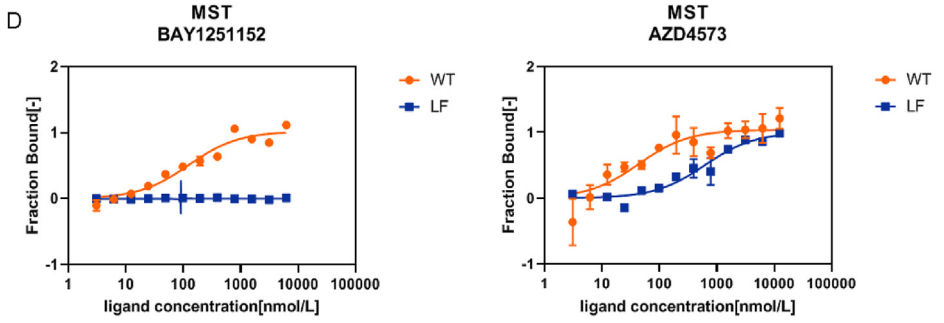

E

Inhibitor-binding constants

	Kd(nmol/L)		IC_{50}(nmol/L)	
	WT	L156F	WT	L156F
BAY1251152	75.31	>10000	12.33	939.5
AZD4573	4.777	594.8	0.8502	60.94

Figure 4 L156F is a common resistance mechanism of CDK9 inhibitors. (A) The 24 h anti-proliferation activity of AZD4573 and THAL-SNS-032 on MOLM13 and MOLM13-BR cells. DRI (drug resistant index) is evaluated based on GI_{50} in parental and resistant cells. (B) The CDK9 degradation potency of THAL-SNS-032 on MOLM13 and MOLM13-BR cells. (C) Inhibition activity against CDK9 WT/cyclinT1 and L156F/cyclinT1 complex proteins measured by ADP-Glo assay. (D) The equilibrium dissociation constants K_d of BAY1251152 and AZD4573 with wild-type and L156F CDK9 kinases determined using micro thermophoresis. (E) Inhibitor-binding constants and inhibition activity summary for BAY1251152 and AZD4573.

structure modeling of BAY1251152 bound to CDK9 variants based on public wild-type CDK9 crystal structure (PDB:6z45) by AutoDock[26] (Fig. 5B). The modeling data showed that, BAY1251152 interacts with CDK9 at the ATP-binding pocket with hydrogen bonds forming between BAY1251152 and Cys106, Glu107, and Asp109 residues in the hinge region. However, in L156F mutant CDK9, the distance between the two benzene rings from F156 and BAY1251152 is less than 2 Å, which could induce steric hindrance and impair the binding of BAY1251152 to CDK9.

To further understand the effect of L156F mutation on CDK9 kinase protein, we then compared the protein sequences across the CDK family. The alignment result revealed that this leucine is conserved in the CDK family (Fig. S3B) and it has been reported that mutation in CDK2 at this conserved position (Leu143 in CDK2) resulted in a dramatic loss in kinase catalytic activity[27]. As CDK kinases share similar protein structures and functions, it indicated that this leucine residue is important for the structure stability and catalytic activity of CDK kinases.

To investigate whether the intrinsic property and kinetics characters of CDK9 were interfered by L156F substitution, we examined the protein thermal stability of the CDK9/cyclinT1 complex. Through differential scanning fluorimetry technique

A

rs1158106390 Position	Gene	Alleles	Change	Amino acid [Codon]	Frequency
chr9:127788247	CDK9	C>A	NM_001261.4:c.466C>A	L [CTT] > I [ATT]	A=0.00006 (1/16760, 8.3KJPN)
		C>T	NM_001261.4:c.466C>T	L [CTT] > F [TTT]	T=0.00007 (1/14050, ALFA)

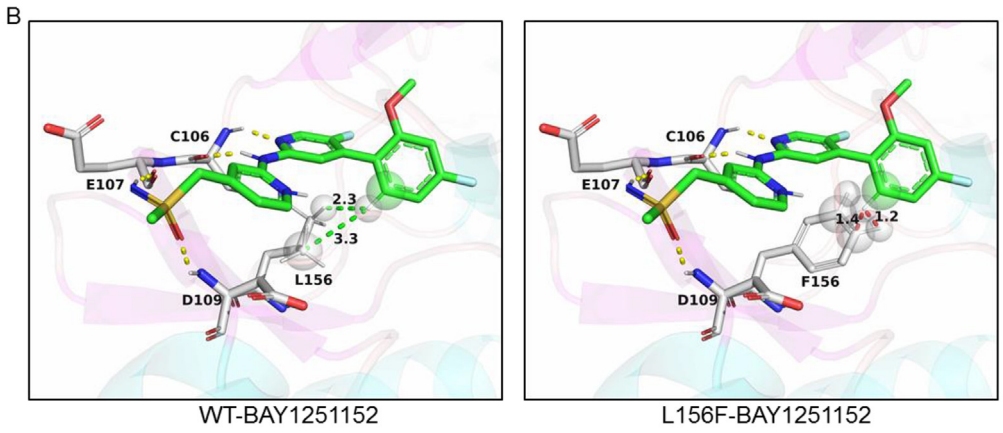

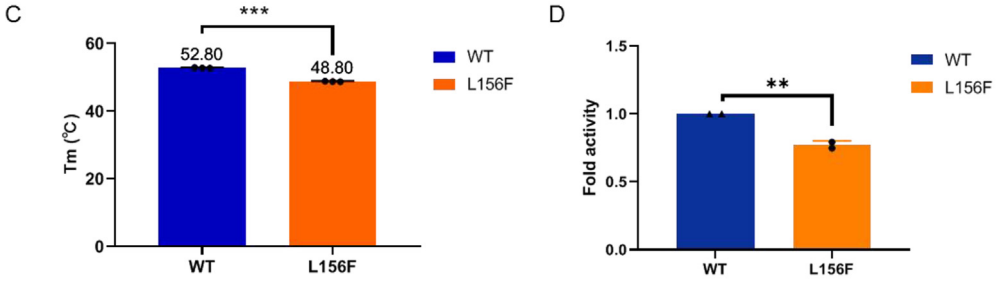

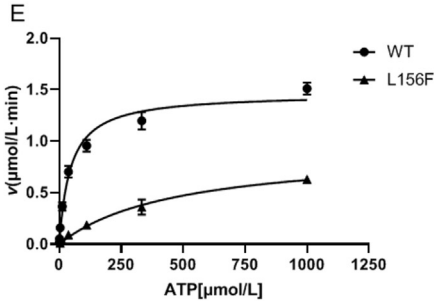

F

Kinase	ATP			
	$K_{m[ATP]}$ μmol/L	K_{cat}, 1/min	V_{max}, 1/min	$K_{cat}/K_{m[ATP]}$, L/μmol·min
WT/CyclinT1	45.11	7.701	1.463	0.1707
L156F/CyclinT1	473.2	4.829	0.9175	0.0102

Figure 5 F156 is a SNP (rs1158106390) disrupt the binding with BAY1251152 and kinase activity. (A) The SNP of CDK9 rs1158106390 was analyzed by dbSNP. (B) Here is the modeling structure of BAY1251152 with CDK9 (PDB ID:6z45) showed in PyMol (The PyMol Molecular Graphics System). L156F mutation was obtained in PyMol using protein mutagenesis wizard function. The modeling was completed by AutoDock. (C) The denatured temperature (T_m) of CDK9 variant proteins were measured by NanoDSF. (D) Comparison of the activity of the WT and L156F kinases. The activity of wild type and mutant CDK9 was determined by *in vitro* kinase assay with saturating ATP and synthesized CTD peptide YSPTSPS as substrate, and the fold activity is normalized to the activity of the wild type CDK9. (E) The activity of WT and L156F CDK9 in the presence of increasing concentration of ATP and saturating CTD peptide. (F) Summary of the kinetic parameters for ATP of WT and L156F CDK9 kinases. Results in the graphs are expressed as means ± SD. ***P*-value < 0.01, ****P*-value < 0.001.

(DSF), we found that the substitution caused a 4-degree downshift of T_m (protein melting temperature), which suggests that L156F mutation perturbs the stability of CDK9/CyclinT1 (Fig. 5C), and this result further verified that the Leu156 is important for the CDK9 complex structural stabilization. Since the mutation is located in ATP binding pocket, we wondered whether the catalytic activity is affected by this substitution. By comparing the activities of WT and L156F kinases by *in vitro* kinase assay with saturated concentrations of ATP and substrate peptide, we found that the L156F activity is slightly weaker than WT kinase (Fig. 5D). When we determined the kinetic parameters of two kinases, the K_m of L156F for ATP increases about 10 folds, which implies that the

affinity of ATP to L156F mutant is reduced with the amino acid change (Fig. 5E). However, the actual effect on ATP binding is likely to be subtle due to the high cellular ATP concentration at millimolar ranges. Further, the V_{max} and the $K_{cat}/K_{m\ [ATP]}$ of L156F also decreased compared to that of wild-type CDK9, suggesting that L156F affects the catalytic activity of CDK9 (Fig. 5F). Consistently, cells harboring CDK9 L156F mutation exhibit reduced proliferation rate and tumor growth rate in mouse models, as CDK9 is necessary to sustain the expression of genes essential for cancer cells, such as MCL1 and MYC.

3.4. *Novel chemical scaffold overcomes SNP-F156 drug resistance*

Because CDK9-L156F renders most of the current CDK9 inhibitors ineffective, we next set out to discover compounds with novel scaffolds that are able to overcome this resistance. Through screening in our in-house compound library consisting over 3000 small molecules, we discovered compound IHMT-CDK9-36 (Fig. 6A, Supporting Information Fig. S4) with potent anti-proliferation activity in both parental and resistant cells (MOLM13 GI_{50} = 2.157 nmol/L, MOLM13-BR GI_{50} = 3.019 nmol/L), meanwhile, the compound exhibited high inhibition potencies for both wild-type and mutant CDK9 (wild-type IC_{50} = 2.766 nmol/L, L156F IC_{50} = 10.15 nmol/L) (Fig. 6B). IHMT-CDK9-36 has similar binding affinities for both WT and L156F, indicating that the interaction of CDK9 with IHMT-CDK9-36 is not significantly influenced by the mutation (Fig. 6C). To better understand the structural basis of CDK9 inhibition by IHMT-CDK9-36, we docked IHMT-CDK9-36 molecule into CDK9 variants, and as the modeling result showed, IHMT-CDK9-36 adopted ATP-competitive binding mode. The pyrilamine ring formed two hydrogen bonds with hinge region residue C106, and methylpiperazine formed a hydrogen bond with E107. In addition, the dihydroisoquinolin interacted with L48 through a hydrogen bond (Fig. 6D). The distance between the phenyl ring of F156 and the dihydroisoquinolin of IHMT-CDK9-36 is enough to accommodate the binding of IHMT-CDK9-36 with CDK9.

Transcriptomic analysis revealed that the total number of differentially expressed genes and biological process enrichment by IHMT-CDK9-36 was similar in both MOLM13 and MOLM13-BR cells (Supporting Information Fig. S5A and S5B). The changes in transcriptional level of MYC and MCL1 are significant in both MOLM13-BR and MOLM13 cells after exposure to IHMT-CDK9-36 (Fig. 6E), which were validated by real-time RT-PCR (Fig. 6F). At the protein level, IHMT-CDK9-36 suppressed the RNA Pol II Ser2 phosphorylation and expression of MCL1/MYC in both resistant and parental cells to similar degrees (Fig. 6G). Additionally, apoptosis was rapidly induced by IHMT-CDK9-36 in resistant cells within 24 h (Fig. 6H). Similar results were obtained in another genome-edited HeLa-CDK9-L156F cell line, in which IHMT-CDK9-36 was also able to overcome the drug resistance conferred by this mutation (Fig. S5C).

As off-target inhibition of other CDK kinases is a major safety concern in the clinical application of CDK9 inhibitors, we next evaluated the cellular selectivity of IHMT-CDK9-36 among other CDK family kinases in MCF7 cells[28]. As the result showed, IHMT-CDK9-36 only inhibited the phosphorylation of CDK9 substrate-Ser2 of RNA Pol II but not those of CDK2/4/6/7 kinases up to 1 μmol/L, which suggests that IHMT-CDK9-36 is a selective CDK9 inhibitor (Fig. 6I). Further, we performed a commercial affinity-based kinome selectivity assay (Supporting file 2) and found that, other than CDK9, IHMT-CDK9-36 also showed binding affinity to CDK7 (Supporting Information Fig. S6A and S6B), which does not accord with cellular selectivity result. Since affinity-based result does not necessarily translate to enzymatic inhibition, we performed *in vitro* kinase assay on CDK7 (Fig. S6C) and the result confirmed that our compound does not affect the catalytic activity of CDK7. In conclusion, both affinity-based kinase profiling and *in vitro* kinase assay showed that IHMT-CDK9-36 achieved moderate selectivity among CDK kinases, which is consistent with the cellular selectivity results.

Finally, the *in vivo* anti-tumor efficacy of IHMT-CDK9-36 was evaluated in xenograft mouse models, and we found that, administrated at 8 mg/kg Q2D, IHMT-CDK9-36 exhibited potent tumor inhibition activity in both MOLM13 and MOLM13-BR tumor models (TGI = 68% in MOLM13, and TGI = 71% in MOLM13-BR) (Fig. 7A, Supporting Information Fig. S7) with suppressed CDK9 signaling pathway in tumor tissues. In contrast, the CDK9 signal pathway was still active after BAY1251152 treatment in MOLM13-BR tumor models, seen from the high level of RNA Pol II Ser2 phosphorylation and sustained expression of MCL1/MYC in tumor tissues (Fig. 7B).

4. Discussion

CDK9 kinase regulates gene transcription by modulating the activity of RNA polymerase II (Pol II), and abnormal overexpression of CDK9 has been observed in many human cancers, in which CDK9 plays critical roles in controlling tumor-related gene transcription mediated by super-enhancers. Therefore, targeting CDK9 provides a feasible therapeutic strategy to suppress the dysregulated transcription process in cancers, thus leading to a decrease of cancer-promoting proteins, such as MCL1 and MYC, and inhibition of cancer cell survival. Preclinical research and clinical trials of selective CDK9 inhibitors have shown promising anti-tumor efficacy in multiple cancer types[7]. However, the potential resistance mechanisms to CDK9 inhibitors are poorly understood. Recently, only one report found that CUL5 ubiquitin ligase mediates resistance to CDK9 inhibitors in lung cancer cells[17]. The canonical acquired resistance mediated through kinase site mutations has not been observed for CDKs inhibitors. As most kinase inhibitors eventually face resistance challenges in clinical use, studies on the potential resistance mechanism of CDK9 inhibitors are essential for their clinical application and new drug development[16].

Since CDK9 inhibitors are still in clinical trials and no information on patient response and drug resistance is available, we developed resistance models in cancer cell lines and found a point mutation responsible for drug resistance. Coincidently, this amino acid substitution is also a reported SNP (single-nucleotide polymorphism) in CDK9 gene that causes the same amino acid change in protein. Previous studies already showed that some SNPs are associated with drug response rate and sensitivity. To find out whether this SNP in CDK9 has any clinical significance, we constructed CDK9-L156F cells using genome editing techniques based on CRISPR/Cas9 and found that edited HeLa-CDK9-L156F cells became insensitive to BAY1251152. Structure modeling and *in vitro* binding results suggest that leu156 is located at the catalytical loop of CDK9 kinase domain with its side chain pointing toward the hydrophobic pocket for ATP binding, L156F disrupts the interaction between CDK9 and the inhibitor due to steric hindrance caused by the relatively larger side chain of

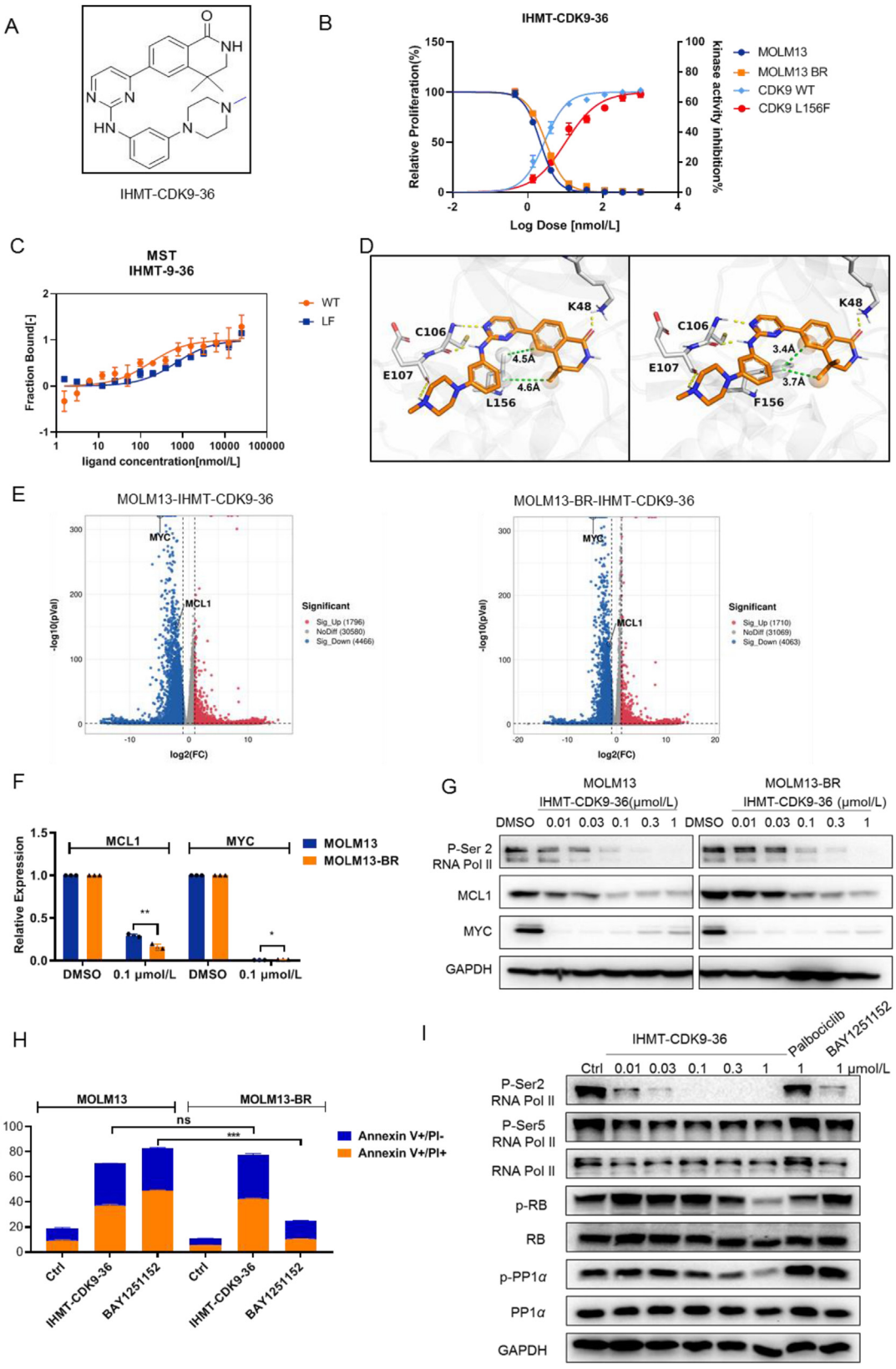

Figure 6 Compound IHMT-CDK9-36 overcome L156F induced resistance. (A) Structure of IHMT-CDK9-36. (B) The anti-proliferation activity and CDK9 kinase inhibition potency of IHMT-CDK9-36 measured by cell Titer-Glo assay and ADP-Glo assay. GI_{50} (nmol/L) and IC_{50} (nmol/L) were fitted by GraphPad Prism8. (C) Binding affinity (K_d) of IHMT-CDK9-36 against CDK9 WT and L156F measured by micro-scale thermophoresis assay. (D) Structural modeling of the interaction of CDK9 variants with IHMT-CDK9-36. (E) The volcano map of differential transcriptomic analysis treated with 0.3 μmol/L IHMT-CDK9-36 for 3 h in MOLM13 (left) and MOLM13-BR cells (right). Changes in transcript

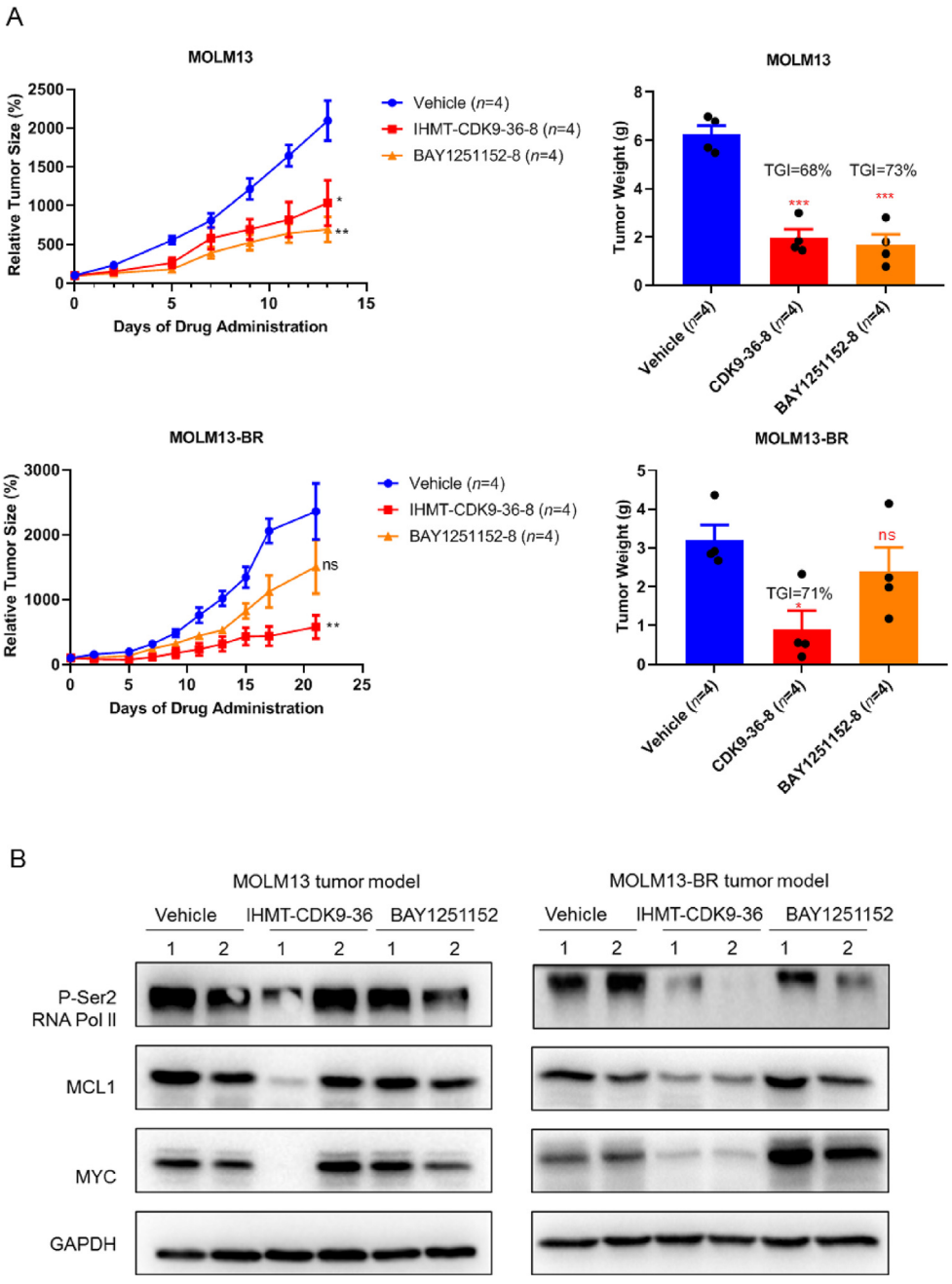

Figure 7 The anti-tumor efficacy of IHMT-CDK9-36 in MOLM13 and MOLM13-BR inoculated mouse models. (A) Measurement of relative tumor size and tumor weight in each group ($n = 4$) after intravenous administrated with IHMT-CDK9-36 or BAY1251152 as 8 mg/kg/Q2D. (B) The p-Ser RNA Pol II, MCL1 and MYC in tumor tissues detected by Western-blot. Results in the graphs are expressed as means ± SD. *P-value < 0.05, **P-value < 0.01, ***P-value < 0.001, and ****$P < 0.0001$, ns, not significant.

phenylalanine. We also found that this conserved leucine is important for CDK9 protein conformation stability and function, as we observed CDK9 L156F protein showed reduced structural stability and catalytic activity compared to the wild-type protein. Contrary to previous knowledge that drug resistance results from mutations causing increased affinity between kinase and ATP, it is unusual what we found here that resistant mutation caused decreased ATP binding affinity.

are defined as not significant (gray), significant up-regulate (red), significant down-regulate (blue). (F) Transcription change of MCL1 and MYC was detected by real time RT-PCR. (G) The CDK9 signaling pathway was compared in MOLM13 and MOLM13-BR cells by Western-blot after exposure to IHMT-CDK9-36 for 2 h. (H) The apoptosis of MOLM13 and MOLM13-BR cells in 24 h induced by 1 μmol/L IHMT-CDK9-36 and BAY1251152 were analyzed by Annexin V/PI staining and flow cytometry. (I) The selectivity of IHMT-CDK9-36 in CDKs family was determined in MCF7 cells. Results in the graphs are expressed as means ± SD. *P-value < 0.05, **P-value < 0.01, ***P-value < 0.001, and ****$P < 0.0001$, ns, not significant.

Since L156F is a reported SNP in human genome, our study suggested that, this amino acid change not only induce acquired resistance to CDK9 inhibitors, but also may provide a potential biomarker for drug response in the clinic as patients carrying this SNP will not respond to most of the CDK9 inhibitors. Currently, we are collecting and screening primary patient cells for this particular genotype to validate our preclinical results.

It is worth noting that, although many CDK mutations have been reported in patients, few of them induced gain- or loss-of-function of CDKs, or resistance to CDK inhibitors. To our knowledge, this is the first time that a mutation in CDK kinase is linked to acquired resistance to inhibitors.

In order to find a novel compound scaffold that could overcome the resistance caused by L156F substitution, we screened our in-house compound library and discovered that IHMT-CDK9-36 showed potent inhibition activity for L156F and suppressed cell viability in cells bearing CDK9-L156F. In addition to ATP-competitive inhibitors, we also explored whether PROTAC inhibitors could overcome the resistance through degradation of CDK9-L156F protein using a reported CDK9 PROTAC inhibitor, THAL-SNS-032. However, this PROTAC only showed weak inhibition on resistance cells and the degradation of CDK9 L156F protein was also decreased, indicating that the binding of CDK9 with SNS-032 (the chemical segment in THAL-SNS-032 responsible for CDK9 binding) was also compromised by CDK9 mutation.

5. Conclusions

Taken together, here we reported an induced point mutation in CDK9 protein that confers resistance to selective CDK9 inhibitors currently in clinical trials. Interestingly, this point mutation coincides with a rare single-nucleotide polymorphism, and thus provides a potential biomarker for future clinical drug response. In addition, we took pharmacological approaches and discovered a novel chemical scaffold that is able to overcome this drug resistance. Together, we believe that this is one of the first studies predicting the possible drug resistance mechanisms of CDK9 inhibitors that are extensively investigated for cancer therapy, and provide an effective novel molecular scaffold of reference value for the development of next-generation inhibitors.

Acknowledgments

We thank Dr. Scott Armstrong at Dana-Farber Cancer Institute (DFCI) of Harvard University for the gifts of MOLM13 cells. This work was supported by the National Natural Science Foundation of China (Grant Nos. 81903650, 32171479, 82103976), the Natural Science Foundation of Anhui Province (Grant Nos. 2008085MH274, 2108085QH377, China), the Collaborative Innovation Program of Hefei Science Center, CAS (Grant No. 2021HSC-CIP014, China), and the CASHIPS Director's Found (Grant Nos. YZJJZX202011, YZJJ2021QN38, China). A portion of this work was supported by the High Magnetic Field Laboratory of Anhui Province.

Author contributions

Chen Hu and Lijuan Shen performed the biological study; Fengming Zhou performed the animal study; Yun Wu synthesized compound IHMT-CDK9-36; Beilei Wang and Chao Wu performed the molecular docking; Aoli Wang and Li Wang analyzed the data; Wenchao Wang, Jing Liu and Qingsong Liu supervised the project and wrote the manuscript. All authors commented and approved the manuscript.

Conflicts of interest

The authors declare no conflicts of interest.

Appendix A. Supporting information

Supporting data to this article can be found online at https://doi.org/10.1016/j.apsb.2023.05.026.

References

1. Sanchez-Martinez C, Gelbert LM, Lallena MJ, de Dios A. Cyclin dependent kinase (CDK) inhibitors as anticancer drugs. *Bioorg Med Chem Lett* 2015;**25**:3420−35.
2. Malumbres M. Cyclin-dependent kinases. *Genome Biol* 2014;**15**:122.
3. Whittaker SR, Mallinger A, Workman P, Clarke PA. Inhibitors of cyclin-dependent kinases as cancer therapeutics. *Pharmacol Ther* 2017;**173**:83−105.
4. Panagiotou E, Gomatou G, Trontzas IP, Syrigos N, Kotteas E. Cyclin-dependent kinase (CDK) inhibitors in solid tumors: a review of clinical trials. *Clin Transl Oncol* 2022;**24**:161−92.
5. Graf F, Mosch B, Koehler L, Bergmann R, Wuest F, Pietzsch J. Cyclin-dependent kinase 4/6 (cdk4/6) inhibitors: perspectives in cancer therapy and imaging. *Mini Rev Med Chem* 2010;**10**:527−39.
6. Rice AP. Roles of CDKs in RNA polymerase II transcription of the HIV-1 genome. *Transcription* 2019;**10**:111−7.
7. Sonawane YA, Taylor MA, Napoleon JV, Rana S, Contreras JI, Natarajan A. Cyclin dependent kinase 9 inhibitors for cancer therapy. *J Med Chem* 2016;**59**:8667−84.
8. Bradner JE, Hnisz D, Young RA. Transcriptional addiction in cancer. *Cell* 2017;**168**:629−43.
9. Li K, You J, Wu Q, Meng W, He Q, Yang B, et al. Cyclin-dependent kinases-based synthetic lethality: evidence, concept, and strategy. *Acta Pharm Sin B* 2021;**11**:2738−48.
10. Abdel-Magid AF. Potential of cyclin-dependent kinase inhibitors as cancer therapy. *ACS Med Chem Lett* 2021;**12**:182−4.
11. Baker A, Gregory GP, Verbrugge I, Kats L, Hilton JJ, Vidacs E, et al. The CDK9 inhibitor dinaciclib exerts potent apoptotic and antitumor effects in preclinical models of MLL-rearranged acute myeloid leukemia. *Cancer Res* 2016;**76**:1158−69.
12. Gregory GP, Hogg SJ, Kats LM, Vidacs E, Baker AJ, Gilan O, et al. CDK9 inhibition by dinaciclib potently suppresses Mcl-1 to induce durable apoptotic responses in aggressive MYC-driven B-cell lymphoma in vivo. *Leukemia* 2015;**29**:1437−41.
13. Wu T, Qin Z, Tian Y, Wang J, Xu C, Li Z, et al. Recent developments in the biology and medicinal chemistry of CDK9 inhibitors: an update. *J Med Chem* 2020;**63**:13228−57.
14. Cheng SS, Qu YQ, Wu J, Yang GJ, Liu H, Wang W, et al. Inhibition of the CDK9-cyclin T1 protein−protein interaction as a new approach against triple-negative breast cancer. *Acta Pharm Sin B* 2022;**12**:1390−405.
15. Barouch-Bentov R, Sauer K. Mechanisms of drug resistance in kinases. *Expert Opin Investig Drugs* 2011;**20**:153−208.
16. Lovly CM, Shaw AT. Molecular pathways: resistance to kinase inhibitors and implications for therapeutic strategies. *Clin Cancer Res* 2014;**20**:2249−56.
17. Kabir S, Cidado J, Andersen C, Dick C, Lin PC, Mitros T, et al. The CUL5 ubiquitin ligase complex mediates resistance to CDK9 and MCL1 inhibitors in lung cancer cells. *Elife* 2019;**8**:e44288.

18. Brookes AJ. The essence of SNPs. *Gene* 1999;**234**:177−86.
19. Ramensky V, Bork P, Sunyaev S. Human non-synonymous SNPs: server and survey. *Nucleic Acids Res* 2002;**30**:3894−900.
20. Piel FB, Steinberg MH, Rees DC. Sickle cell disease. *N Engl J Med* 2017;**376**:1561−73.
21. Deng N, Zhou H, Fan H, Yuan Y. Single nucleotide polymorphisms and cancer susceptibility. *Oncotarget* 2017;**8**:110635−49.
22. Zeron-Medina J, Wang X, Repapi E, Campbell Michelle R, Su D, Castro-Giner F, et al. A polymorphic p53 response element in KIT ligand influences cancer risk and has undergone natural selection. *Cell* 2013;**155**:410−22.
23. Thomas E, Jana H, Philipp E, Benjamin H, Armin L, Rüdiger H, et al. ABL single nucleotide polymorphisms may masquerade as BCR-ABL mutations associated with resistance to tyrosine kinase inhibitors in patients with chronic myeloid leukemia. *Haematologica* 2008;**93**:1389−93.
24. Ota M, Tahara T, Otsuka T, Jing W, Nomura T, Hayashi R, et al. Association between receptor interacting serine/threonine kinase 2 polymorphisms and gastric cancer susceptibility. *Oncol Lett* 2018;**15**:3772−8.
25. Love MI, Huber W, Anders S. Moderated estimation of fold change and dispersion for RNA-seq data with DESeq2. *Genome Biol* 2014;**15**:550.
26. Morris GM, Huey R, Lindstrom W, Sanner MF, Belew RK, Goodsell DS, et al. AutoDock4 and AutoDockTools4: automated docking with selective receptor flexibility. *J Comput Chem* 2009;**30**:2785−91.
27. Elphick LM, Lee SE, Child ES, Prasad A, Pignocchi C, Thibaudeau S, et al. A quantitative comparison of wild-type and gatekeeper mutant cdk2 for chemical genetic studies with ATP analogues. *Chembiochem* 2009;**10**:1519−26.
28. Wells CI, Vasta JD, Corona CR, Wilkinson J, Zimprich CA, Ingold MR, et al. Quantifying CDK inhibitor selectivity in live cells. *Nat Commun* 2020;**11**:2743.